Mansoura Engineering Journal

Volume 48 | Issue 6 Article 8

October 2023

Study the Structural Behavior of Back-to-Back Cold-Formed Steel Columns with Different Types of Web Stiffeners

Mahmoud Elnagar
Assistant Professor, Civil Engineering Department, Faculty of Engineering, Menofia University, Shebeen El-kom, Egypt

Boshra A. El-Taly
Professor of Structitural Analysis and Mechanics, Civil Engineering Department, Faculty of Engineering, Menofia University, Shebeen El-kom, Egypt

Dalia N. Elmenshawy
Demostrator, Civil Engineering Department, Faculty of Engineering, Menofia University, Shebeen El-kom, Egypt, dalianor@sh-eng.menofia.edu.eg

Ghada M. Hekal
Associate Professor of Structitural Analysis and Mechanics, Civil Engineering Department, Faculty of Engineering, Menofia University, Shebeen El-kom, Egypt

ORIGINAL STUDY

Study the Structural Behavior of Back-to-back Cold-formed Steel Columns With Different Types of Web Stiffeners

Mahmoud Elnagar, Boshra A. El-Taly, Dalia N. Elmenshawy*, Ghada M. Hekal

Civil Engineering Department, Faculty of Engineering, Menoufia University, Shebin El-kom, Egypt

Abstract

The study investigated the behavior of six cold-formed steel (CFS) columns with lipped channel and various web stiffener configurations under axial compression forces until failure. The research compared the experimental results with Finite Element (FE) analysis conducted using the Abacus program, analyzing the ultimate load, axial shortening, and failure mode. The columns were made by brake-pressing CFS sheets with a nominal thickness of 1.5 mm and joining identical members with self-drilling screws to form an I-shaped section with web and edge stiffeners. The test specimens were 1000 mm long and compressed between fixed base and top hinged end conditions. The study found a good correlation between the experimental and numerical results. The validated Finite Element model was used for a parametric study of CFS columns with various web stiffener configurations and dimensions. The results showed that stiffening the web increased the ultimate load and improved the columns' structural behavior. The study also found that the column with a trapezoidal-shaped stiffener had the highest ultimate load.

Keywords: Back-to-back, Cold-formed steel channel column, Edge web stiffener, Finite element modeling, Intermediate web stiffener, Lipped channel

1. Introduction

Cold Formed Steel; CFS sections are manufactured at lower temperatures than hot rolled sections, resulting in minimal shrinkage. This process produces a stronger and more visually appealing product with precise dimensions and corners, making it ideal for exterior applications. CFS is commonly used in construction to produce structural shapes and panels with high accuracy and consistency.

Numerous research studies have focused on comprehending the structural behavior of CFS column sections, as well as identifying the factors that influence their capacity, strength, and failure modes. One key area of interest for researchers has been enhancing the capacity and efficiency of CFS column sections by incorporating stiffeners, which has proven to increase section capacity and improve structural behavior.

Li and Young (2023) tested 20 simply supported CFS columns under concentric compression. The experimental results in terms of loading capacity, failure mode and load versus shortening response were obtained and then employed to calibrate the finite element model. El-Taly and Fattouh (2022) employed numerical analysis using the ANSYS software to investigate sixteen CFS channel columns with different combinations of edge and web stiffeners under axial compression. They analyzed the ultimate load, stiffness, ductility, and energy absorption in relation to column parameters. Liu and colleagues (Liu et al., 2018) performed axial load tests and analysis on cold-formed rectangular steel columns with large and thick walls, distinguishing between direct and indirect types based on the

Received 26 March 2023; revised 21 June 2023; accepted 23 June 2023.
Available online 18 October 2023

* Corresponding author at: Civil Engineering Department, Faculty of Engineering, Menoufia University, Shebin El-kom, 32515, Egypt. Fax: (048) 1110222.
E-mail address: dalianor@sh-eng.menofia.edu.eg (D.N. Elmenshawy).

https://doi.org/10.58491/2735-4202.3073

forming processes and highlighting the variations in yield and ultimate strengths. Aruna and colleagues (Aruna et al., 2019) experimentally investigated cold-formed built-up closed sections with intermediate web stiffeners under axial compression, comparing the column strengths obtained from finite element analysis with those calculated using the AISI specification for CFS structures. Ziqi He and colleagues (He et al., 2023) examined the performance of composite section members with V-shaped and Σ-shaped web stiffeners in 44 experimental tests involving built-up sections of different lengths under axial and eccentric compression loading. Their findings demonstrated improved loading capacity and restricted local buckling behavior. Badr and colleagues (Badr et al., 2022) focused on studying the distributed load capacity of CFS sections in lightweight buildings through testing nine frames until failure and utilizing a validated finite element model to explore various characteristics affecting the load capacity of CFS built-up sections. Gurupatham and colleagues (Gurupatham et al., 2022) investigated the post-buckling behavior and axial capacity of thin-walled steel stiffened single-channel sections and back-to-back stiffened channel sections, highlighting the role of stiffeners in enhancing axial capacity. Ananthi and Ashvini (2019) conducted an extensive experimental, theoretical, and numerical investigation on plain and lipped CFS built-up stub channel columns with different provisions of stiffeners. Ghannam (2017) examined the axial load capacity of innovative CFS built-up stub columns, comparing different design codes and highlighting the need for revision in certain codes. Huang and colleagues (Huang et al., 2018) presented a simplified analytical model for determining the critical stress of distortional buckling in lipped channel-sections with stiffened CFS web, emphasizing their superior resistance to local buckling. Roy and colleagues (Roy et al., 2022) investigated screw-fastened back-to-back built-up aluminum alloy slender columns under axial compression, assessing various design standards and their accuracy in predicting axial strengths.

The buckling behavior of the CFS column is governed by various parameters such as cross-sectional geometry, dimensions, web stiffeners and flange stiffeners. The experimental investigation covers testing on back-to-back CFS lipped channel columns. Six CFS short columns were factory-made and tested up to failure to understand their structural behavior. These specimens are chosen with the same shape of edge stiffener, Lipped channel (LC). The main difference between the tested specimens was the shape of web stiffener (WS) to study the effect of this on the behavior of the built-up columns. Nonlinear FE modeling was performed for the tested columns using Abacus, and their results were compared with the experimental results. The verified FE model was used to conduct a parametric study. Eighteen models, divided into four groups, were investigated to study some main parameters that effect on the structural behavior of CFS columns.

The objective of this study was to conduct experimental and numerical investigations on the behavior of six CFS columns with lipped channel and different web stiffener configurations under axial compression forces until failure. The study aimed to make several contributions to the field, including: (1) evaluating the impact of adding an edge web stiffener in conjunction with the main middle web stiffener on the overall structural behavior of CFS lipped channel columns, (2) determining the optimal length of the web stiffener for a given middle web stiffener shape, by considering the stiffener length to the web length ratio, and (3) determining the optimal length of the edge web stiffener for a given middle web stiffener shape, by considering the edge stiffener length to the web length ratio. By investigating these key factors, the study aimed to provide valuable insights into enhancing the structural performance of CFS lipped channel columns.

2. Experimental work

In order to investigate the structural behavior of CFS columns, six columns with a length of 1000 mm were fabricated and tested until failure. Each column was formed by joining two single sections in the longitudinal direction of the column using self-tapping screws. The screws were spaced nominally at 50 mm, with a smaller spacing of 25 mm provided at the edges of the columns to prevent any problematic slipping between the sections. This approach was based on the work of El-Taly and El-shami (El-Taly and El-shami, 2021), while Ting and colleagues (Ting et al., 2017) studied the effect of screw spacing. The screw diameter and length were 4.8 mm and 12.5 mm, respectively.

The columns had a flange width of 60 mm and a lip length of 16 mm. The web was equipped with various shaped stiffeners, including triangular, trapezoidal, and rectangular, with a total length of 180 mm and the same cross-sectional area of 489 mm^2.The specimens were categorized and labeled based on the type of edge and web stiffeners used. For instance, a column with no web stiffener was

labeled as 'C', while a column with a web stiffener was labeled as 'WS'. The edge stiffener shape was indicated by 'LC' for lipped channel column, while the web stiffener shapes were 'Tg.' for a triangle, 'Rg.' for a rectangle, and 'Tz.' for a trapezoidal shape. The column dimensions satisfied the geometric limitations of NAS, 2007, which are available for a single section only. Based on the single section, a built-up section was selected. Fig. 1 shows the measured cross-sectional dimensions, the type of web stiffeners used, and the locations of the screws on the cross-section. Table 1 presents the identification numbers and descriptions of the six specimens tested in this study. Detailed dimensions of the columns, all in millimeters, are provided in Table 2.

To ensure accurate alignment and connection of the two channel sections, steel plates were welded to the ends of the columns. A load jack was used to apply the axial load, and the self-drilling screws were arranged along the column according to the method described by Roy and colleagues (Roy et al., 2018). The top end plate, known as the loading plate, was selected to be very rigid with a thickness of 15 mm to distribute the load evenly and combine the two channels into an I-section. The bottom end plate, known as the base plate, was 30 mm thick and used to fasten the two channels from the bottom end, fulfilling the fixed end condition. Fig. 2 illustrates the load jack and the arrangement of self-drilling screws along the column.

To examine the material properties, the researchers conducted tensile coupon tests using coupons taken from the web in the longitudinal direction. The results showed that the yield stress F_y, 250 MPa, the initial Young's modulus E, 19 4448.7 MPa, the ultimate tensile strength F_u, 360 MPa, and the corresponding strain ϵ_u, 0.053.

To conduct the tests on the specimens, each column was placed inside a steel frame in the laboratory, as depicted in Fig. 3. The verticality of the column was carefully adjusted using a hydrometer to ensure that the column was perfectly vertical and that the load was applied vertically, thereby

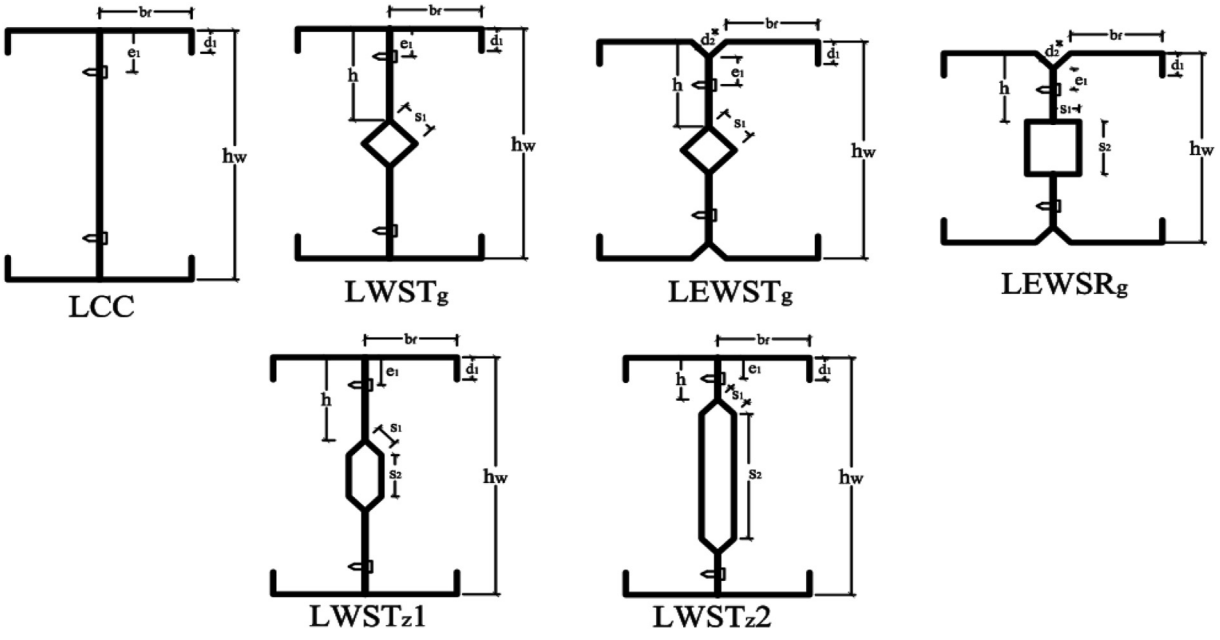

Fig. 1. The details of the cross sections for tested columns.

Table 1. Column description.

No.	Col. ID	Description
1	**LCC**	Control specimen with no web stiffener.
2	**LWST$_g$**	Lipped channel with triangle web stiffener.
3	**LEWST$_g$**	Lipped channel with triangle and end web stiffeners.
4	**LEWSR$_g$**	Lipped channel with rectangle and end web stiffener.
5	**LWST$_z$1**	Lipped channel with trapezoidal web stiffener (stiffener = $h_o/3$).
6	**LWST$_z$2**	Lipped channel with trapezoidal web stiffener (stiffener = $2h_o/3$).

Table 2. Tested column dimensions.

No.	Col. ID	Dimensions, mm								
		L	b_f	d_1	d_2	S_1	S_2	h	h_w	e_1
1	LCC				_	_	_	180	180	30
2	$LWST_g$				_	24	_	66	165.9	20
3	$LEWST_g$	1000	60	16	16	24	_	50	156.6	20
4	$LEWSR_g$				16	17	38	38	136.7	15
5	$LWST_Z1$				_	15	30	60	171.2	20
6	$LWST_Z2$				_	15	90	30	171.2	15

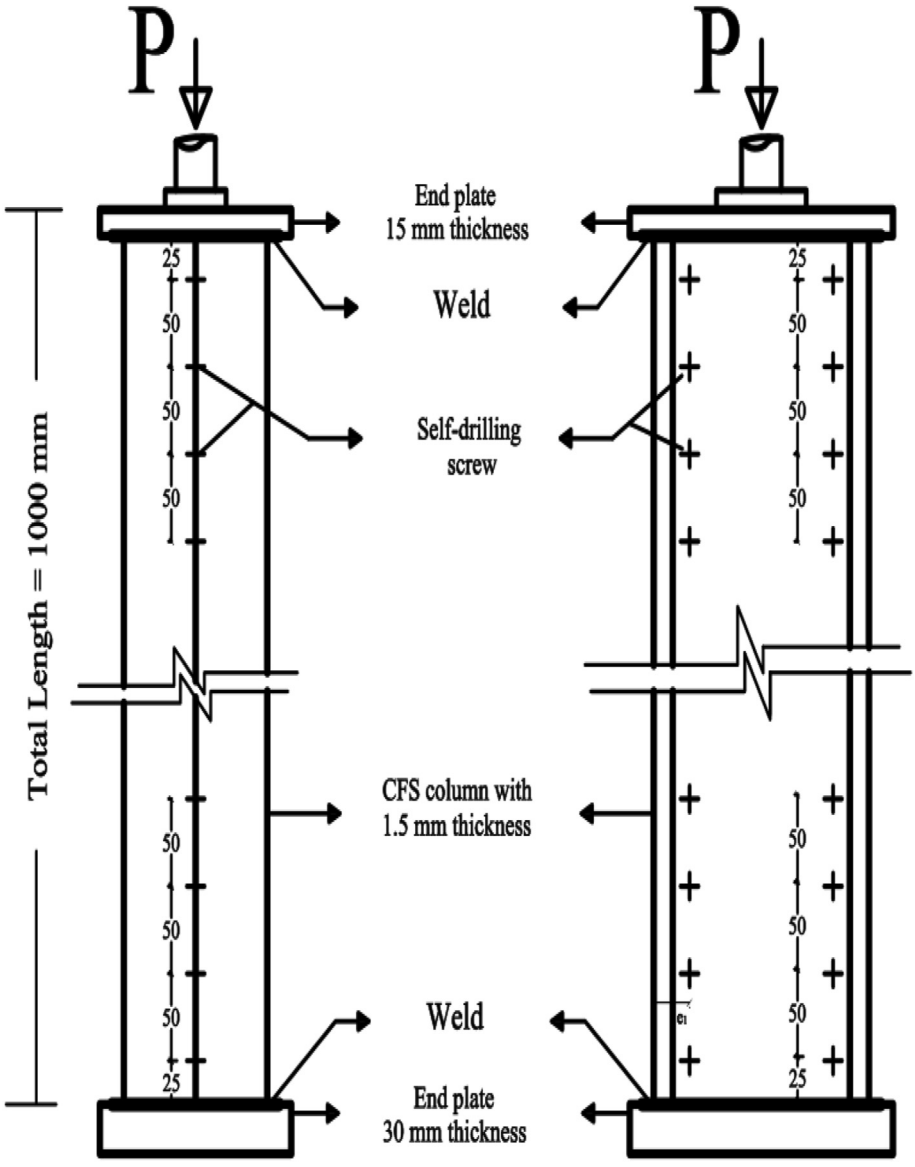

Fig. 2. The arrangement of screws.

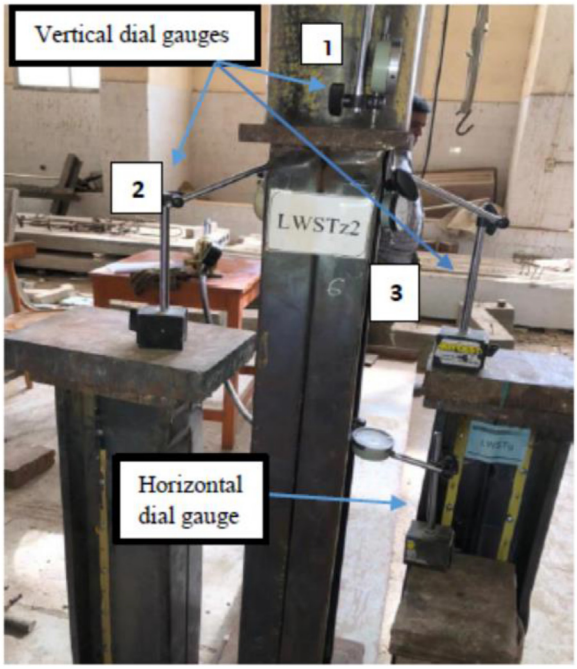

Fig. 3. Test arrangement.

ensuring accurate results. Four Dial Gauges were installed at designated locations on the column to measure the test results, with three being positioned vertically at the top to record axial shortening and one being installed horizontally at mid-length to detect local buckling. The tests were conducted at a loading rate of 5 kN, and the deformation value, either axial displacement or local buckling, was recorded at each load.

The column specimens were loaded from zero load, and the readings of the four dial gauges were recorded. The load was increased gradually at a rate of 5 kN, and the readings of the four dial gauges were taken for each load step until the column failed. The capacity of the column until failure was noted when the column could no longer resist the load. Three dial gauges were placed at the top to read the axial shortening of the column under axial compression (See Fig. 3).

The first dial gauge was beside the load cell, the second was under the top end plate from the right side, and the third was from the left side. The average of these recorded readings was calculated to give the total axial displacement due to the ultimate load. For each dial gauge, the reading at every loading stage was recorded, and the displacement was calculated by subtracting the values from the initial reading of the dial gauge (before loading). The behavior of the test specimens was observed throughout the testing. It was noted that for most of the test specimens, no conclusive data for local buckling could be derived from the dial gauges readings. The test results are summarized in Table 3.

3. Finite element modeling

To gain a better understanding of the behavior of CFS columns under compression loads, a finite element (FE) modeling approach was employed using the Abacus program. The study conducted a comparative analysis between the results obtained from FE analysis and experimental investigations. Evaluation was based on factors such as failure modes, load–displacement graphs, and ultimate load. In the current models, the column was represented using shell elements (S4R) based on the center line dimensions of the cross-section, Anbarasu and colleagues (Anbarasu et al., 2014), while the two end plates were modeled using solid elements (C3D8R) with an element size of (15 × 15 × 15) mm. For the column, a fine mesh size was utilized to closely match the experimental results. Multiple mesh sizes were tested to accurately simulate the experimental conditions.

In the FE modeling process, different mesh sizes were evaluated to determine the accuracy of the results. Initially, a large mesh size of 30 mm was used, but it yielded inaccurate results and had a longer solution time. Mesh enhancement was then performed by using finer meshes of 2.5, 5, 10, and 15 mm. The results obtained with the 10 mm and 15 mm meshes aligned well with the experimental

Table 3. The short results of tested columns.

Col. No	1	2	3	4	5	6
Col. ID	LCC	$LWST_g$	$LEWST_g$	$LEWSR_g$	$LWST_z1$	$LWST_z2$
Cross-Section		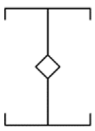	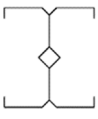	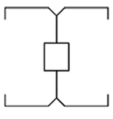	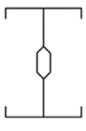	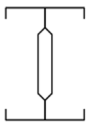
Ultimate Load	120 kN	165 kN	185 kN	195 kN	235 kN	215 kN
Displacement	3.5 mm	8.71 mm	4.1 mm	5.65 mm	5.56 mm	8.7 mm
Failure mode	Local Buckling					

results. Eventually, a mesh size of 15 mm was chosen due to the small differences between the results of the 10 mm and 15 mm models. The mesh configuration of the column is depicted in Fig. 4. Grade 37 steel material was employed for the sheets in the study.

Regarding boundary conditions, all degrees of freedom were restricted for the top and bottom plates, except for the displacement at the loading plate (top surface) in the direction of the applied load. Fig. 5 illustrates the boundary conditions of the two end plates and the pressure load.

The loading process consisted of two stages. In the first stage, a linear perturbation with buckling type and unit load was applied to obtain the buckling modes and eigenvalues of the column. In the second stage, a nonlinear analysis was conducted using a separate model with two differences: the procedure type was set as general with Static Riks type, and the load value was equal to the eigenvalue obtained in the first stage. The Risk method, suitable for analyzing nonlinear collapse behavior, was employed to incrementally apply the load using the available Abacus option. To represent the

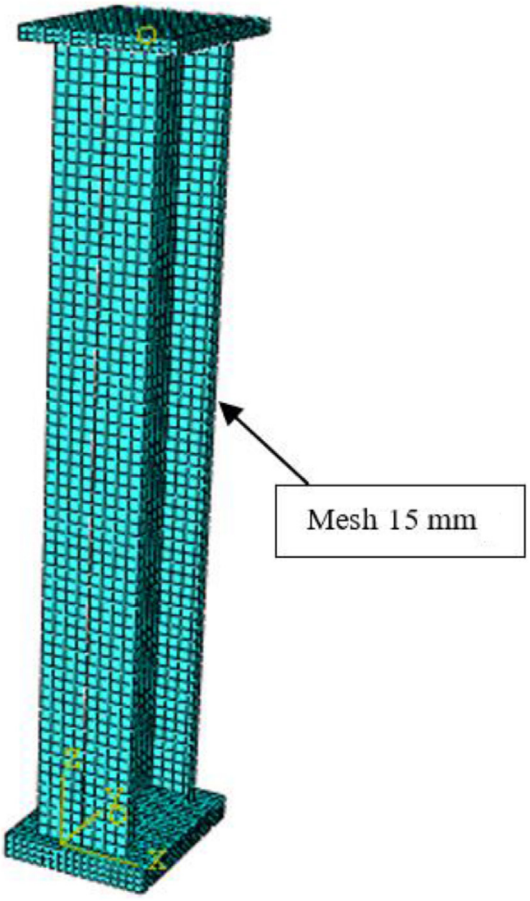

Fig. 4. The column mesh.

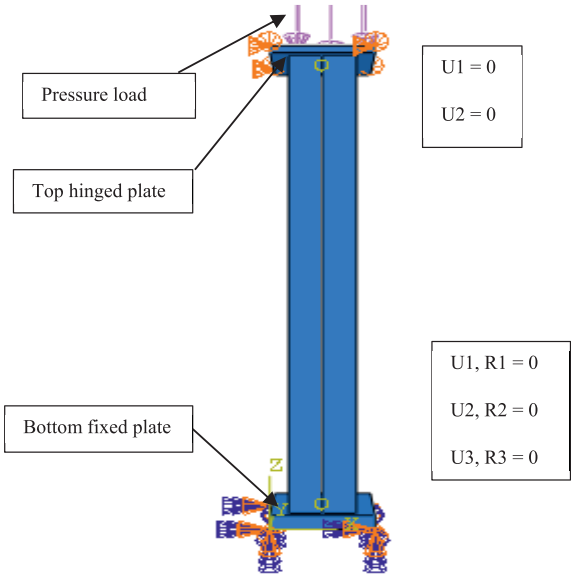

Fig. 5. End conditions and applied pressure loads.

connections between the two channels and between the column and the two end plates, different types of interactions were defined. The interaction between the two channels in the CFS lipped channel columns was defined using a tie interaction at the bolt locations. This approach was selected based on its ability to provide more accurate results that closely matched the experimental behavior. However, when attempting to consider the interaction between the channels away from the bolt locations, the obtained results did not accurately reflect the expected behavior. To investigate this further, a comparison was made between the defined interaction at bolt locations and the inclusion of interaction away from these locations. It was observed that including the interaction away from the bolt locations led to discrepancies between the simulated results and the experimental behavior. Specifically, the ultimate load increased by 15.75%, while the axial displacement increased by 10.8% compared with the experimental results. Shell-to-solid coupling was selected to accurately simulate the interaction between the column and the two end plates, emulating the experimental setup.

4. Results and discussion

To validate the numerical analysis and assess the reliability of the finite element models, the results obtained from the models were compared side-by-side with the experimental results. This comparison aimed to determine if the FE models accurately represented the behavior of the real column samples. Additionally, the ultimate load leading to column failure was solely determined from the

experimental tests and was also included in the evaluation.

4.1. Ultimate load

The ultimate load, representing the maximum load the specimens could bear, was determined experimentally for all tested specimens. Fig. 6 illustrates the load–displacement (P-D) curves of the tested specimens. The stiffness (K) was calculated as the ratio of the load at the end of the linear stage to the corresponding displacement. The ductility ratio (D_r) was defined as the displacement at the ultimate load divided by the displacement at the end of the linear zone. Energy absorption (E_n) was determined as the area under the P-D curve (El-Taly and El-shami, 2021). These calculated values are summarized in Table 4.

To verify the FE model, a comparison was made between the experimental and FE results. Differences were analyzed for the ultimate loads obtained from experimental work (P_{Exp}) and finite element analysis (P_{Num}), as well as for the load–displacement relationships. Table 5 and Fig. 7 present the difference in ultimate loads between the CFS columns obtained experimentally and numerically using the finite element model. The results indicated a good agreement between the experimental and numerical findings.

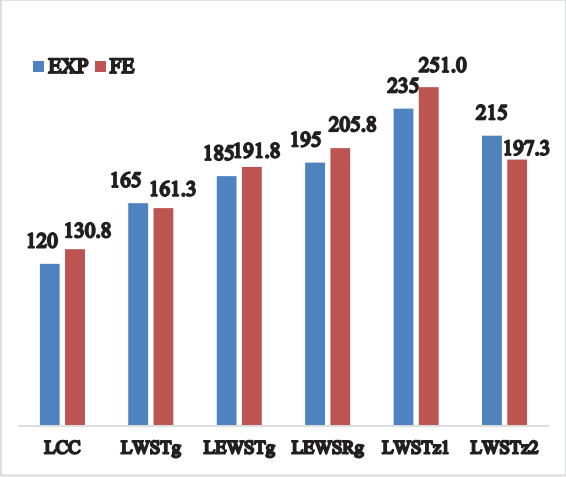

Fig. 6. P–D curve of tested columns (experimental).

Table 5. Ultimate load comparison.

Col. No	Col. ID	Ultimate Load(kN)		Difference (%)
		Exp.	Num.	
1	LCC	120	130.85	8.29
2	$LWST_g$	165	161.26	2.27
3	$LEWST_g$	185	191.83	3.56
4	$LEWSR_g$	195	205.8	5.25
5	$LWST_z1$	235	251	6.37
6	$LWST_z2$	215	197.25	8.26
Mean Difference				**5.67**

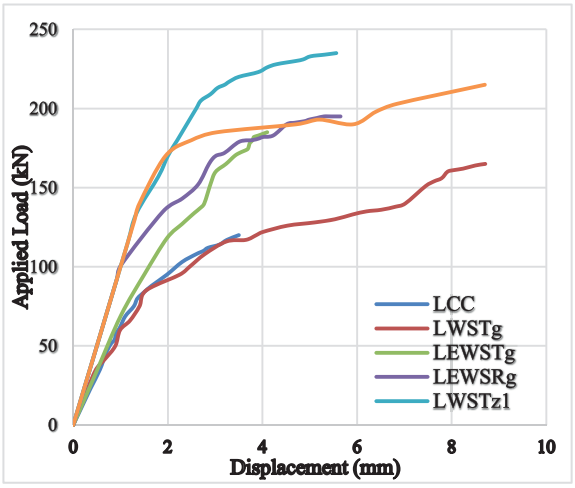

Fig. 7. Exp. and Num. Ultimate load values in kN.

In comparing the results, it was observed that columns with web stiffeners exhibited increased column capacity compared with the control column specimen (LCC), given the same perimeter and column length. Different types of web stiffeners led to varying column capacities, with each column achieving an ultimate load higher than the control column. Among the specimens, it was found that using a trapezoidal web stiffener with a length equal to 1/3 of the total web height (specimen 5, LWSTz1) provided the highest ultimate load. However, increasing the web stiffener length to match the

Table 4. Experimental results.

Col. No	Col. ID	End linear zone		Ultimate		Stiffness (kN/mm)	Dr	En (kN.mm)
		P(kN)	D(mm)	P(kN)	D(mm)			
1	**LCC**	23	0.364	120	3.5	63.19	9.62	277.98
2	**$LWST_g$**	36	0.5	165	8.71	72.00	17.42	987.31
3	**$LEWST_g$**	69	1.004	185	4.1	68.73	4.08	543.18
4	**$LEWSR_g$**	101	1.01	195	5.65	100	5.6	811.25
5	**$LWST_z1$**	134	1.34	235	5.56	100	4.15	961.92
6	**$LWST_z2$**	140	1.40	215	8.7	100	6.21	1492.89

total web length (specimen 6, LWSTz2) did not yield an advantage and resulted in a decreased ultimate load compared with specimen 5. Overall, the difference between the experimental and FE results for CFS columns with different web stiffeners did not exceed 10%.

4.2. Axial-shortening

The load–displacement relationships for the tested specimens were obtained through experimental and numerical analysis, as shown in Fig. 8. Overall, a good agreement was observed between

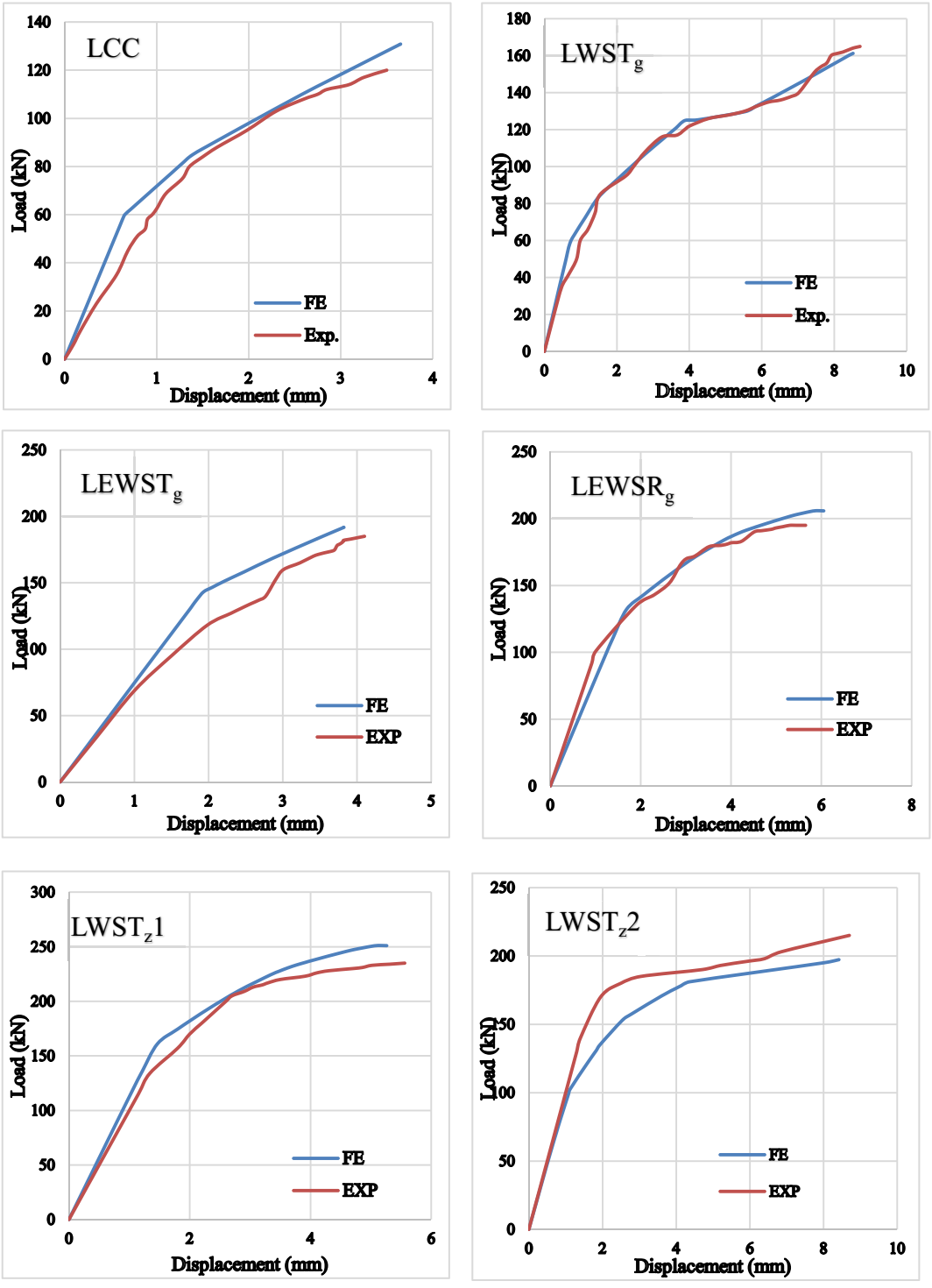

Fig. 8. Exp. and Num. Load-displacement curves.

Table 6. Axial-shortening comparison.

No.	Col. ID	Displacement (mm)		$D_{Exp.}/D_{Num.}$
		Exp.	Num.	
1	LCC	3.5	3.65	0.96
2	$LWST_g$	8.71	8.52	1.02
3	$LEWST_g$	4.1	3.82	1.07
4	$LEWSR_g$	5.65	6.05	0.93
5	$LWST_z1$	5.56	5.26	1.06
6	$LWST_z2$	8.7	8.42	1.03

the experimental (Exp.) and numerical (Num.) results, which were further compared in Table 6.

Both the experimental and numerical relationships indicated that the load–displacement behavior followed a linear trend in the initial stage. However, after reaching the point of local buckling of the steel sheets, the behavior became nonlinear. This observation was consistent in both the experimental and numerical analyses.

4.3. Failure mode

Fig. 9 depicts the failure shape observed in the experimental tests as well as the simulation of the finite element models, along with the buckling mode. Since the tests were stopped upon the first occurrence of failure, no conclusive damage was observed. The buckling mode observed in both the experimental (Exp.) tests and FE analysis was Local Buckling (LB). This observation is consistent with the findings of Ziqi He and colleagues (He et al., 2023). The failure of the columns was attributed to stress concentration at the top of the columns under loading. Specifically, the failure occurred at the top third of each specimen.

The results in Table 4 reveal important findings regarding the tested columns. Specimen LWSTz1, which featured a trapezoidal web stiffener, exhibited the highest ultimate load with a 95.8% increase compared with the control specimen (LCC). On the other hand, specimen LWSTz2, with an increased stiffener length, demonstrated a 30.3% capacity improvement compared with specimen LWSTg. This indicates that the failure load changes with variations in the stiffener length while keeping the same stiffener type. However, increasing the stiffener length without batten plates resulted in a 9.3% decrease in the ultimate load compared with specimen LWSTz1. The control specimen (LCC) had the lowest values for ultimate load (P), stiffness (K), and energy absorption (En). In contrast, specimen LWSTz2 exhibited the highest energy absorption. Additionally, specimen LWSTg had the highest ductility ratio (Dr), while specimen LEWSRg had the lowest. Overall, these findings demonstrate that the use of an edge web stiffener generally improved the structural behavior of the CFS columns. Among the various shapes studied, the trapezoidal web stiffener proved to be the most effective in enhancing column performance in the experimental work.

5. Parametric study

In this section, a parametric study was conducted using the verified FE model. The study consisted of four groups, each containing four or five columns with varying shapes or dimensions of web stiffeners. Figs. 10–13 illustrate the columns in each group. The parameters investigated were the presence of an edge web stiffener and changes in web stiffener shape and length. Table 7 provides a description of the investigated columns. All models had constant dimensions, including a length (L) of 4000 mm, a cross-sectional area of 1424 mm^2, a perimeter (B) of 720 mm, and a sheet thickness (t) of 2 mm. According to the Egyptian code ECP-205, these columns are classified as short columns based on their length and cross-sectional dimensions. The lipped flange had a width (bf) of 120 mm and a lip length (d1) of 40 mm in all models, satisfying the geometric limitations of lipped channel sections. The dimensions for all models are provided in Table 8. The models were subjected to compression loads until failure under two different end conditions: fixed at the bottom and hinged at the top to allow axial displacement. The material properties and nonlinear parameters were consistent across all models. The parametric study aimed to extend the findings of the experimental work.

The first group (Group 1) consisted of four columns: one without web stiffeners and three models with different web stiffener shapes (Triangle, Tg; Rectangle, Rg; and Trapezoidal, Tz). The second group (Group 2) included the same models as Group 1 but with an additional edge web stiffener. The third group (Group 3) comprised five columns with edge and trapezoidal web stiffeners. The main difference among the models in this group was the web stiffener length relative to the web length, while the edge web stiffener length remained constant. The fourth group (Group 4) consisted of five columns with edge and trapezoidal web stiffeners. In this group, the main difference was the edge web stiffener length relative to the web length, while the web stiffener length remained constant.

For all models, an element size of 25 × 25 × 25 mm was chosen for the loading and bottom plates, while an element size of 50 × 50 × 2 mm was suitable for

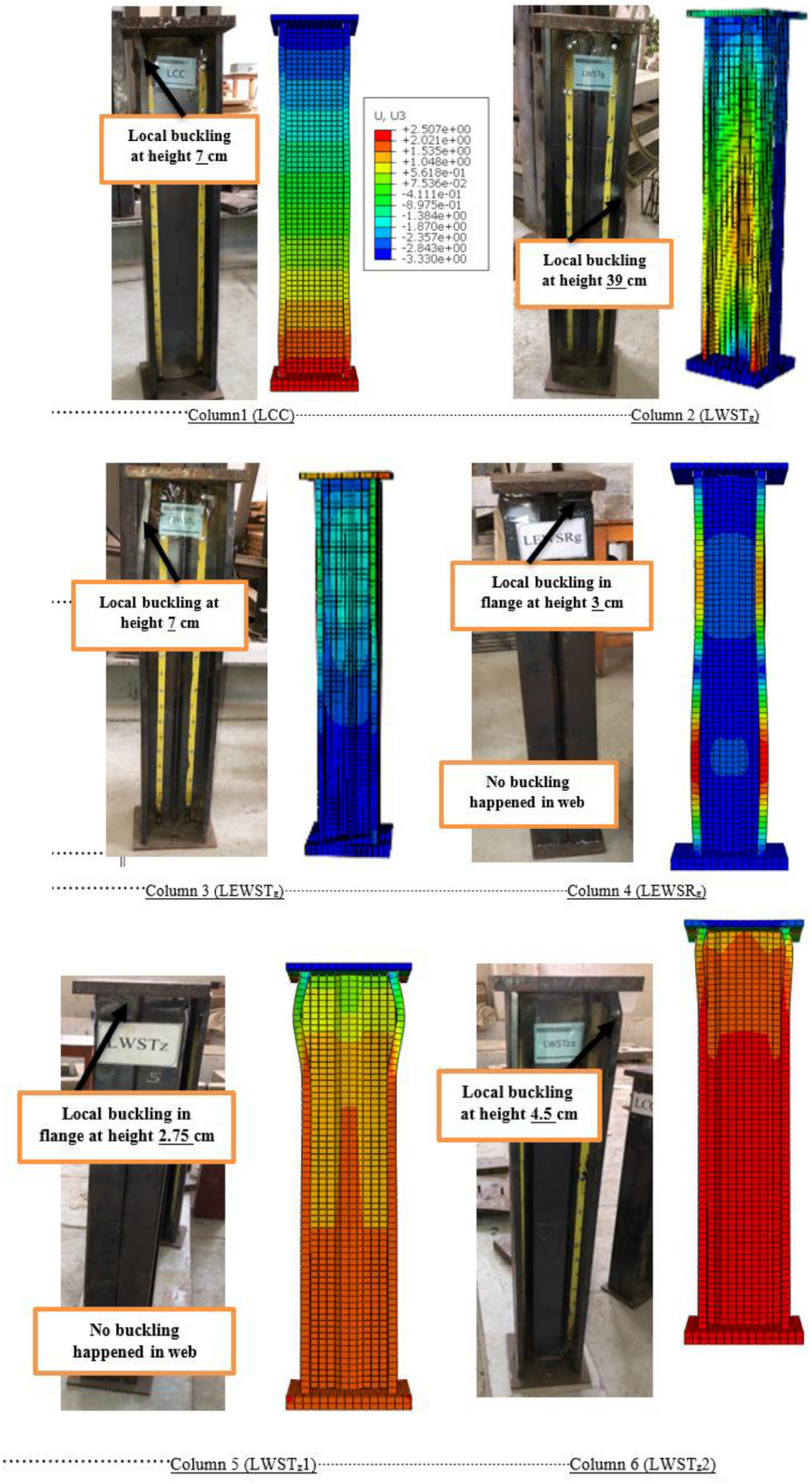

Fig. 9. Exp. and FE. Failure shape.

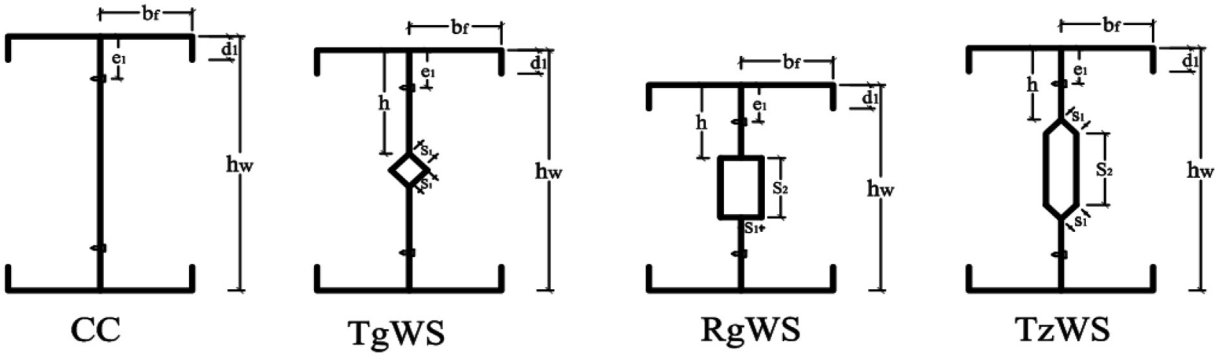

Fig. 10. Group 1, columns with no edge web stiffener.

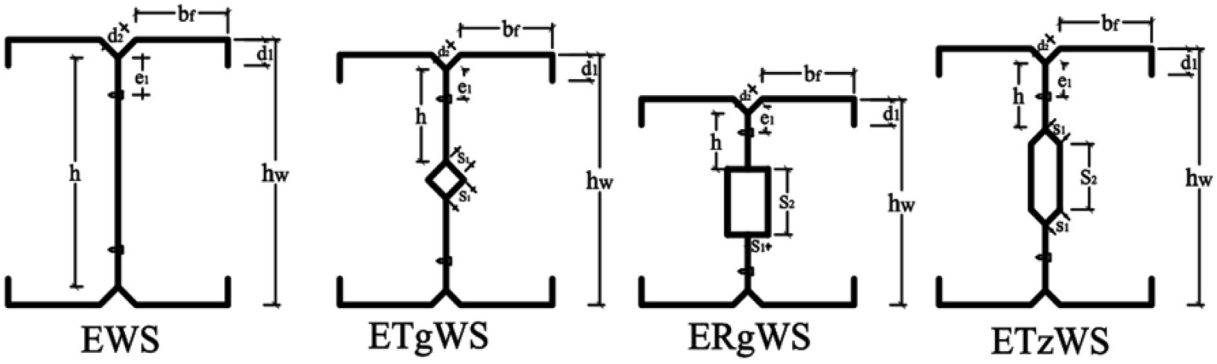

Fig. 11. Group 2, columns with edge web stiffener.

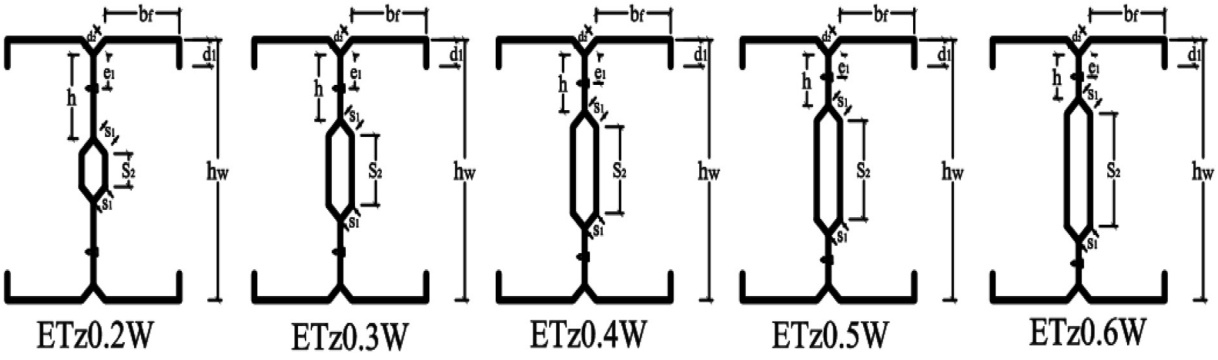

Fig. 12. Group 3, columns with different web stiffener lengths.

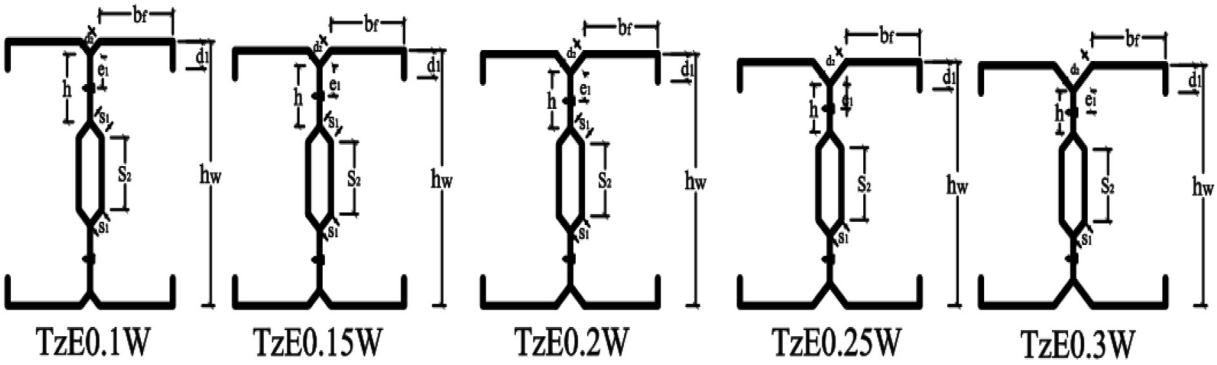

Fig. 13. Group 4, columns with different edge web stiffener lengths.

Table 7. Labels of the investigated columns.

	No.	Group	Code	Description
G1		1	**CC**	Control column with no web stiffener.
		2	**T_gWS**	With triangle web stiffener at middle length.
	With no edge web stiffener	3	**R_gWS**	With rectangle web stiffener at middle length.
		4	**T_zWS**	With trapezoidal web stiffener at middle length.
		1	**EWS**	Control column with edge web stiffener.
		2	**ET$_g$WS**	With triangle web stiffener at middle length and edge web stiffener.
G2	**With edge web stiffener**	3	**ER$_g$WS**	With rectangle web stiffener at middle length and edge web stiffener.
		4	**ET$_z$WS**	With trapezoidal web stiffener at middle length and edge web stiffener.
		1	**ET$_z$-0.2W**	Trapezoidal and edge stiffeners, stiffener length = 0.225 the web length.
		2	**ET$_z$-0.3W**	Trapezoidal and edge stiffeners, stiffener length = 0.33 the web length.
G3	**With different web stiffener lengths**	3	**ET$_z$-0.4W**	Trapezoidal and edge stiffeners, stiffener length = 0.425 the web length.
		4	**ET$_z$-0.5W**	Trapezoidal and edge stiffeners, stiffener length = 0.5 the web length.
		5	**ET$_z$-0.6W**	Trapezoidal and edge stiffeners, stiffener length = 0.6 the web length.
		1	**T$_z$E-0.1W**	Trapezoidal and edge stiffeners, edge web stiffener length = 0.1 the web length.
		2	**T$_z$E-0.15W**	Trapezoidal and edge stiffeners, edge web stiffener length = 0.15 the web length.
G4	**With different edge web stiffener lengths**	3	**T$_z$E-0.2W**	Trapezoidal and edge stiffeners, edge web stiffener length = 0.2 the web length.
		4	**T$_z$E-0.25W**	Trapezoidal and edge stiffeners, edge web stiffener length = 0.25 the web length.
		5	**T$_z$E-0.3W**	Trapezoidal and edge stiffeners, edge web stiffener length = 0.3 the web length.

Table 8. The column models dimensions, mm.

Group	No.	Code	d_2	S_1	S_2	h	h_w	e_1
G1	1	**CC**	_	_	_	400	400	80
	2	**T_gWS**	_	40	110	160	376.57	80
	3	**R_gWS**	_	35	110	110	330	50
	4	**T_zWS**	_	35	_	110	379.5	50
G2	1	**EWS**	30	_	_	340	382.43	70
	2	**ET$_g$WS**	30	40	_	130	359	60
	3	**ER$_g$WS**	30	30	94	93	322.43	45
	4	**ET$_z$WS**	30	30	94	93	364.85	45
G3	1	**ET$_z$-0.2W**	30	20	50	125	370.71	60
	2	**ET$_z$-0.3W**		25	84	103	367.78	50
	3	**ET$_z$-0.4W**		30	110	85	364.85	40
	4	**ET$_z$-0.5W**		40	120	70	359	35
	5	**ET$_z$-0.6W**		40	160	50	359	25
G4	1	**T$_z$E-0.1W**	20	20	80	120	376.57	60
	2	**T$_z$E-0.15W**	30			110	370.71	55
	3	**T$_z$E-0.2W**	40			100	364.85	50
	4	**T$_z$E-0.25W**	50			90	359	45
	5	**T$_z$E-0.3W**	60			80	353.14	40

the columns. Grade 37 steel was used for the sheet material, consistent with the experimental models. The ultimate load was determined for all models, and Figs. 14–17 depict the load–displacement curves (P-D) for each group. The stiffness (K), ductility ratio (Dr), and energy absorption (En) were calculated and summarized in Table 9. Figs. 18–21 display the failure shapes of each column under compression load for all models in each group. Finally, Fig. 22 provides a comprehensive comparison of the columns in terms of ultimate load, stiffness, ductility, and energy absorption, offering a clear overview of the different parameters that significantly influence the structural behavior of the CFS columns.

In Group 1, where no edge web stiffener was present, the model CC reached a total load of 156.84 kN with a displacement of 0.469 mm in the linear zone. It failed due to local buckling at an ultimate load of 349.36 kN and a displacement of 2.69 mm. The ultimate load decreased with increasing displacement, reaching 305.1 kN at

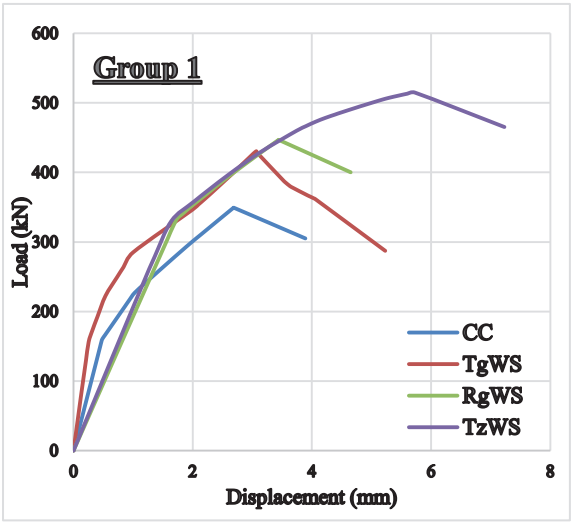

Fig. 14. Load-displacement curves of Group 1.

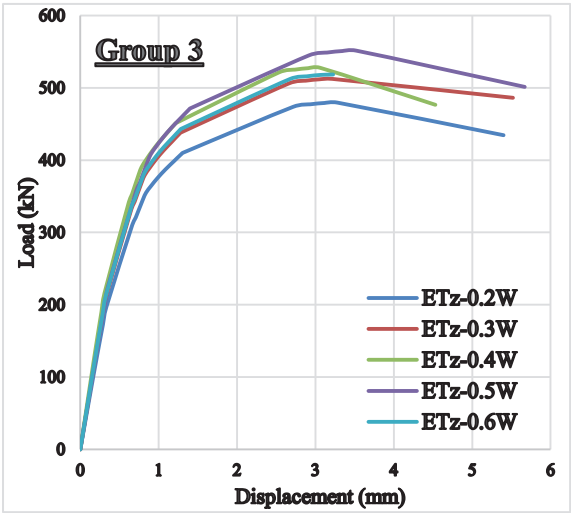

Fig. 16. Load-displacement curves of Group 3.

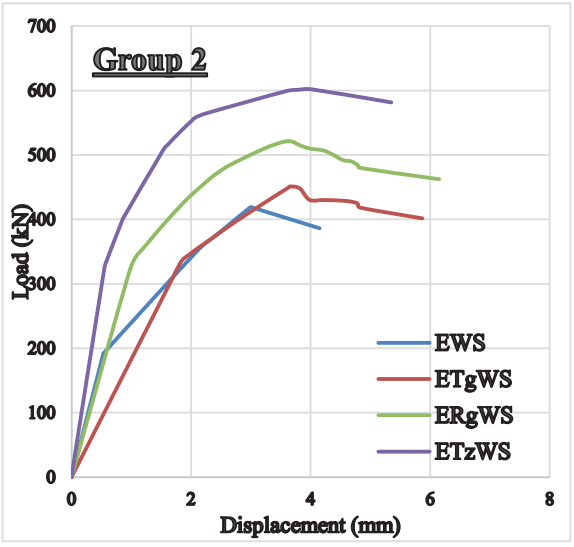

Fig. 15. Load-displacement curves of Group 2.

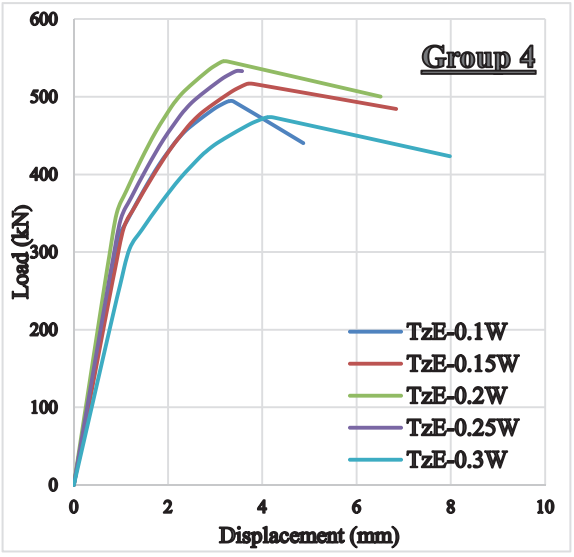

Fig. 17. Load-displacement curves of Group 4.

3.89 mm. The stiffness (K) was 334.41 kN/mm, the ductility ratio (Dr) was 5.74%, and the energy absorption (En) was 1018.95 kN mm. The model TgWS failed at an ultimate load of 430.56 kN and a displacement of 3.07 mm. The ultimate load decreased with displacement, reaching 287.3 kN at 5.23 mm. The values of K, Dr, and En were 620.38 kN/mm, 14.69%, and 1688.28 kN mm, respectively. Using the triangle web stiffener improved the structural behavior of the CFS columns, increasing the column capacity by 23.24% and the stiffness, ductility ratio, and energy absorption by 85.5, 155.9, and 65.7%, respectively. The model RgWS failed at an ultimate load of 446.96 kN and a displacement of 3.44 mm, resulting in a 27.94% increase in ultimate load compared with the control model. The energy absorption increased by 44.39%, but the stiffness decreased by 42.67%. The model TzWS failed at an ultimate load of 514.84 kN and a displacement of 5.73 mm, showing a 47.37% increase in ultimate load compared with the control model. The energy absorption increased by 177.6%, but the stiffness and ductility ratio decreased by 39.8% and 39.2%, respectively. Among the models in Group 1, the model TgWS exhibited the highest values for both K and Dr, while the model TzWS had the highest values for P and En. This indicates that the model with a trapezoidal shape of web

Table 9. Results of parametric study (load in kN and displacement in mm).

Group No.	Code	End linear zone		Ultimate		Stiffness (kN/mm)	Dr	En (kN.mm)	Failure mode
		P	D	P	D				
G1	CC	156.84	0.469	349.36	2.69	334.41	5.74	1018.95	
	T_gWS	129.66	0.209	430.56	3.07	620.38	14.69	1688.28	
	R_gWS	333.58	1.74	446.96	3.44	191.71	1.98	1471.28	Local buckling
	T_zWS	330.15	1.64	514.84	5.73	201.31	3.49	2828.31	
G2	EWS	192.74	0.54	419.23	3.00	356.93	5.56	1286.44	
	ET_gWS	337.16	1.86	451.06	3.66	181.27	1.97	1962.24	
	ER_gWS	334.11	1.03	520.71	3.69	324.38	3.58	2574.13	Local buckling
	ET_zWS	330.46	0.57	601.92	4.01	579.75	7.04	2721.03	
G3	ET_z-0.2W	196.81	0.33	479.59	3.28	596.39	9.94	2216.49	
	ET_z-0.3W	210.27	0.33	512.38	3.21	637.18	9.73	2457.41	
	ET_z-0.4W	216.57	0.31	527.75	3.06	698.61	9.87	2018.91	Local buckling
	ET_z-0.5W	226.32	0.36	551.5	3.52	628.67	9.78	2671.43	
	ET_z-0.6W	212.74	0.33	518.41	3.23	644.67	9.79	2539.43	
G4	T_zE-0.1W	316.95	0.944	493.95	3.39	335.75	3.59	1893.87	
	T_zE-0.15W	331.47	1.06	516.59	3.81	312.71	3.59	2929.33	
	T_zE-0.2W	349.96	0.91	545.41	3.27	384.57	3.59	2974.81	Local buckling
	T_zE-0.25W	342.04	0.995	533.06	3.57	343.76	3.59	3203.12	
	T_zE-0.3W	303.74	1.18	473.37	4.24	257.41	3.59	3118.6	

stiffener is the most efficient, with a 47.37% increase in column capacity compared with the CC model, and improvements of 19.57% and 15.19% compared with the TgWS and RgWS models, respectively. These findings are consistent with the experimental work.

In Group 2, which includes columns with an edge web stiffener, the control model (EWS) reached a

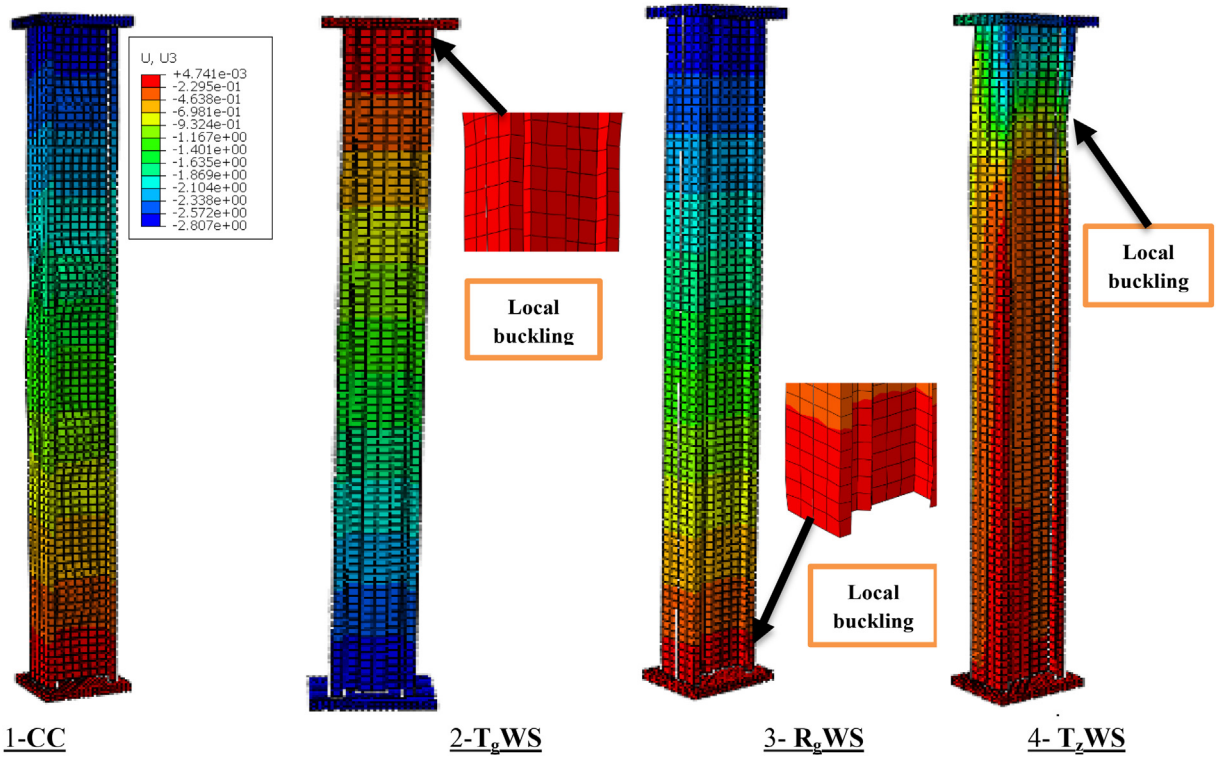

Fig. 18. Failure shapes of models in Group 1.

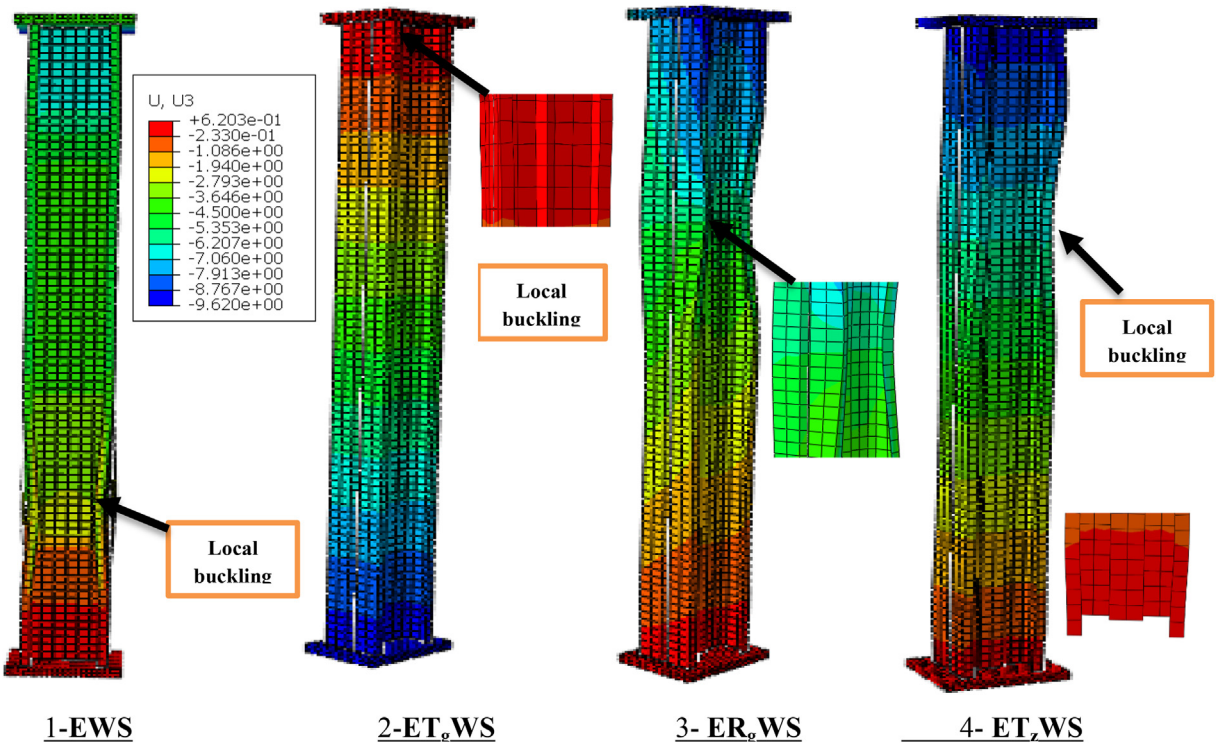

Fig. 19. Failure shapes of models in Group 2.

total load of 192.72 kN and a displacement of 0.54 mm in the linear zone. It failed at an ultimate load of 419.23 kN and a displacement of 3.0 mm. The stiffness (K) was 356.93 kN/mm, the ductility ratio (Dr) was 5.56%, and the energy absorption (En) was 1286.44 kN mm. The use of an edge web stiffener resulted in a 20% increase in column capacity, a 26.25% increase in energy absorption, and a 6.73%

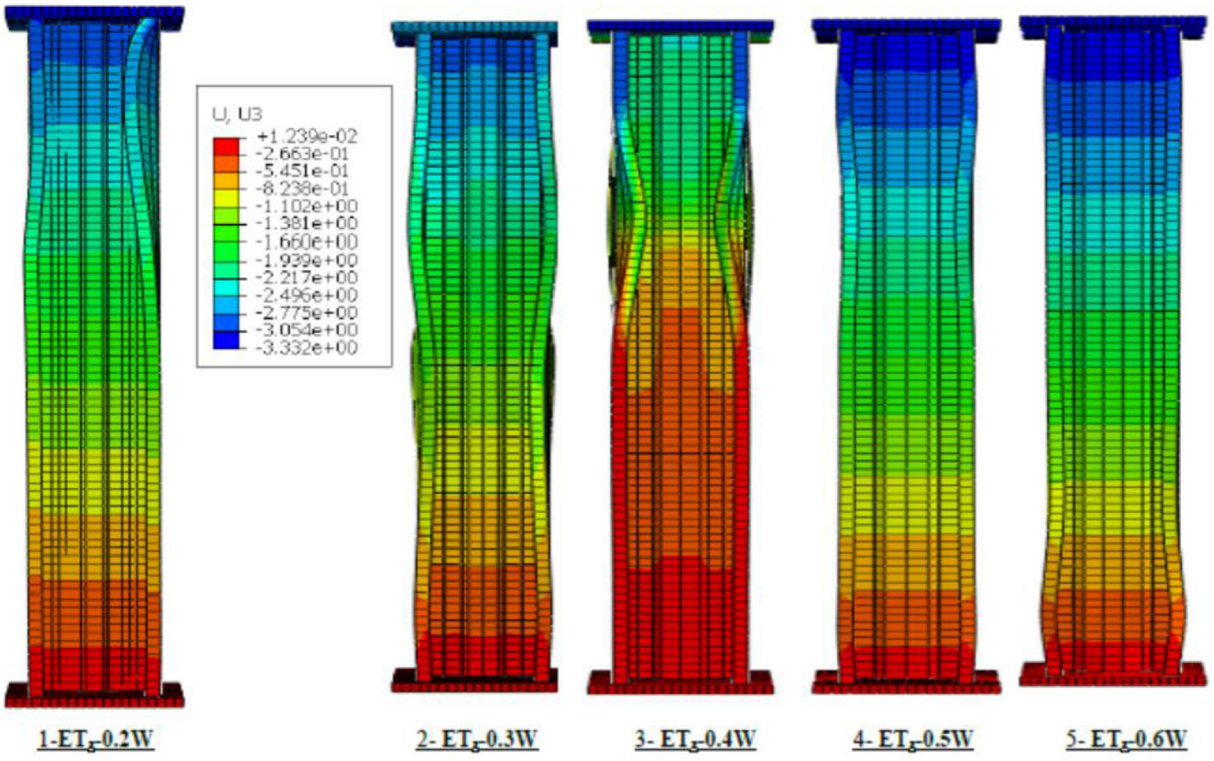

Fig. 20. Failure shapes of models in Group 3.

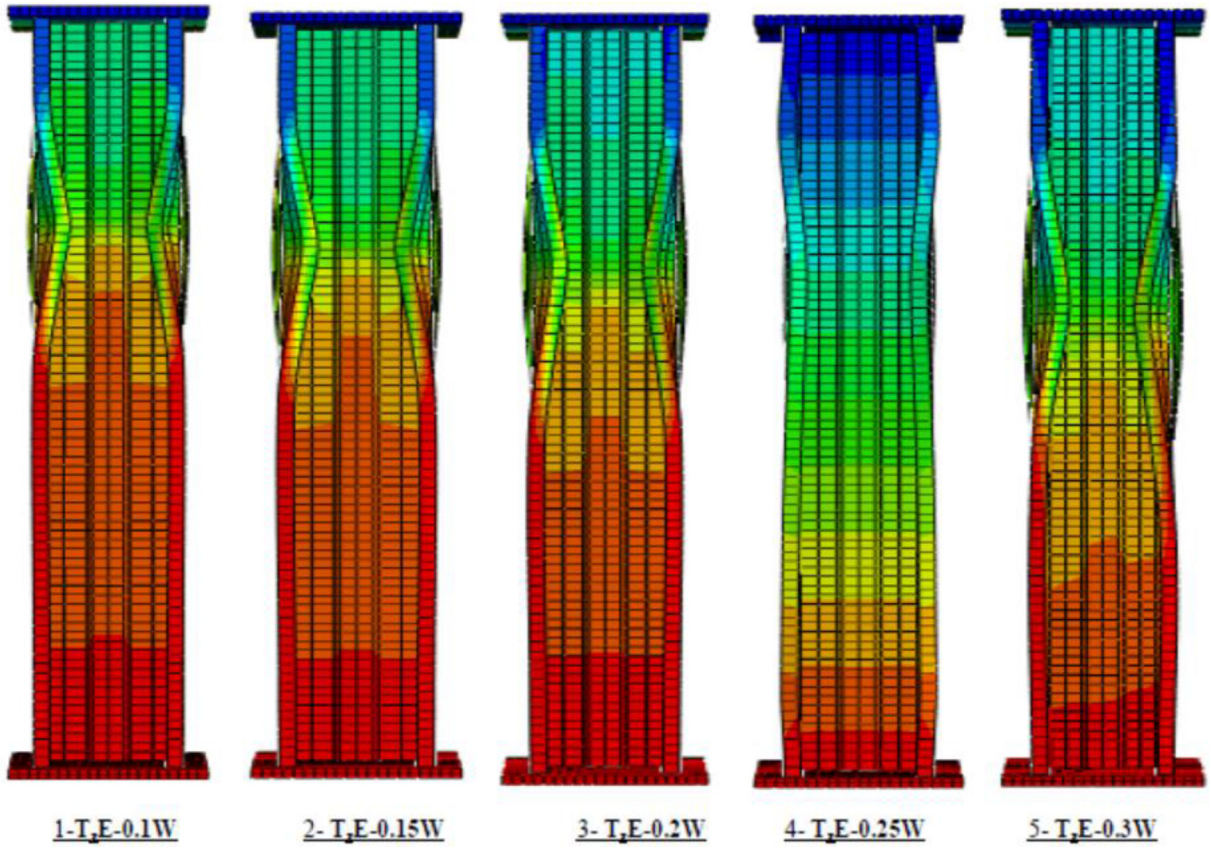

Fig. 21. Failure shapes of models in Group 4.

increase in stiffness compared with the control model (CC) in Group 1. The model ETgWS had an ultimate load of 451.06 kN and a displacement of 3.66 mm at failure. Comparing it to EWS, the triangle web stiffener increased column capacity and energy absorption by 7.6% and 52.53%, respectively, but decreased stiffness and ductility ratio by 49.21% and 64.56%, respectively. Comparing ETgWS to TgWS in Group 1, ETgWS had higher load capacity and energy absorption, with increases of ~4.76% and 16.23%. The model ERgWS had an ultimate load of 520.71 kN and a displacement of 3.69 mm at failure, showing a 24.2% increase in failure load and a 52.47% increase in energy absorption compared with EWS. Compared with RgWS in Group 1, ERgWS had increases of 16.5% in ultimate load and 75% in energy absorption. The model ETzWS had an ultimate load of 601.92 kN and a displacement of 4.01 mm at failure, showing increases of 43.58% in failure load and 111.52% in energy absorption compared with EWS. Compared with TzWS in Group 1, ETzWS had a 16.9% increase in ultimate load, but a 3.4% decrease in energy absorption. In Group 2, the model EWS had the lowest values for P and En, while the model ETzWS had the highest values for all computed results: P, K, Dr, and En. Comparing all models in Group 1 and Group 2, it is observed that the use of an edge web stiffener improved the structural behavior of CFS columns overall. Additionally, the comparison shows that the ETzWS model is the most effective among all models in both groups. This finding aligns with the experimental work for models LEWSTg and LEWSRg.

In Group 3, which includes columns with different web stiffener lengths, the reference model (ETz-0.2 W) failed at a load of 479.59 kN and a displacement of 3.28 mm, with stiffness (K), ductility ratio (Dr), and energy absorption (En) values of 596.39 kN/mm, 9.94%, and 2216.49 kN mm, respectively. The model ETz-0.3 W had an ultimate load of 512.38 kN and a displacement of 3.21 mm at failure, with calculated values of K, Dr, and En equal to 637.18 kN/mm, 9.73%, and 2457.41 kN mm, respectively. Comparing ETz-0.3 W to the reference model (ETz-0.2 W), increasing the web stiffener length from 0.225 to 0.3 of the web resulted in a 6.84% increase in ultimate load, as well as increases of 6.84% in stiffness (K) and 10.9% in energy absorption (En). The model ETz-0.4 W had an ultimate load of

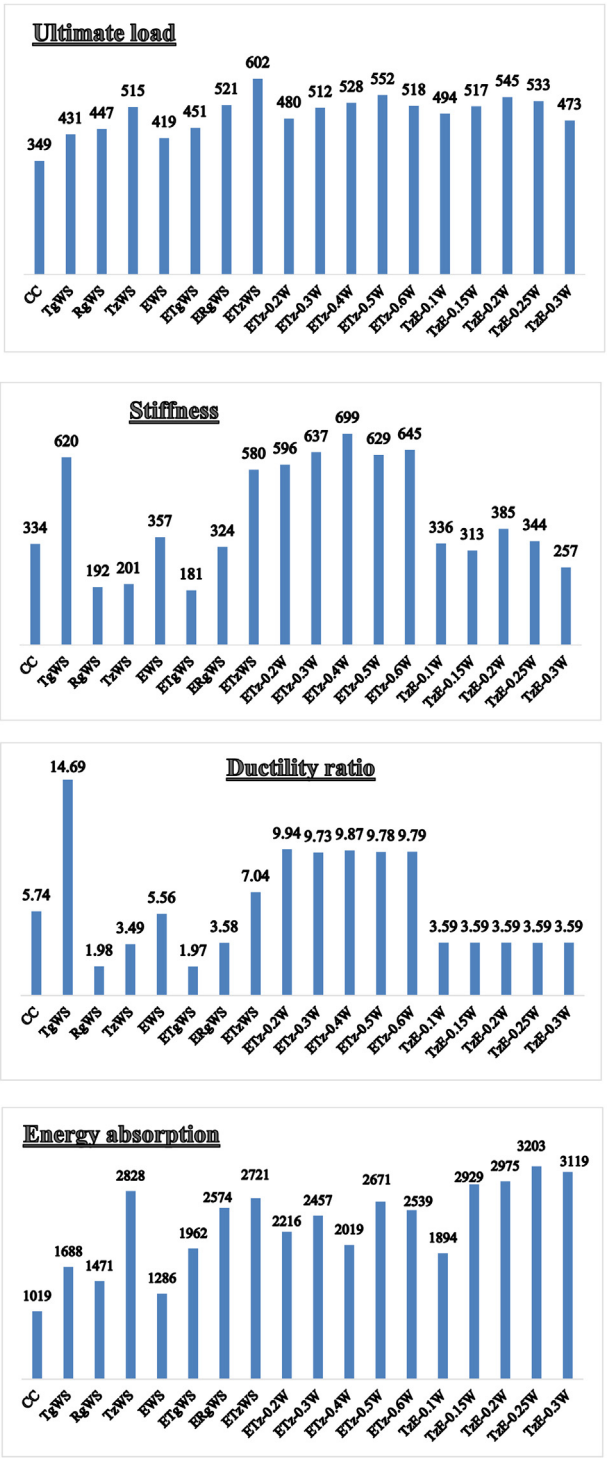

Fig. 22. Structural behavior of studied models of the parametric study.

527.75 kN and a displacement of 3.06 mm at failure, with K, Dr, and En values of 698.81 kN/mm, 9.87%, and 2018.91 kN mm, respectively. Comparing ETz-0.4 W to the reference model, increasing the web stiffener length from 0.225 to 0.4 of the web resulted in a 10.04% increase in ultimate load, a 17.14% increase in stiffness (K), but an 8.91% decrease in energy absorption (En). The model ETz-0.5 W had an ultimate load of 551.5 kN and a displacement of 3.52 mm at failure. Comparing it to the reference model, increasing the web stiffener length from 0.225 to 0.5 of the web resulted in a 15% increase in ultimate load, as well as increases of 5.41% in stiffness (K) and 20.53% in energy absorption (En). The model ETz-0.6 W had an ultimate load of 518.41 kN and a displacement of 3.23 mm at failure. Comparing it to the reference model, increasing the web stiffener length from 0.225 to 0.6 of the web resulted in an 8.1% increase in ultimate load, as well as increases of 8.1% in stiffness (K) and 14.57% in energy absorption (En). However, comparing ETz-0.6 W to ETz-0.5 W showed that increasing the web stiffener length from 0.5 to 0.6 of the web resulted in a 6% decrease in ultimate load and a 4.94% decrease in energy absorption, but a 2.55% increase in stiffness. All models had nearly the same value for the ductility ratio and failed due to local buckling. Overall, the structural behavior of the CFS columns improved with increasing the web stiffener length. However, it is not desirable for the ratio between the stiffener length and the web length to exceed 0.5, as this ratio yielded the highest values for ultimate load (P), stiffness (K), ductility ratio (Dr), and energy absorption (En), as seen in model ETz-0.5 W. When this ratio exceeds 0.5, all of these values decrease.

Group 4 consists of columns with different edge web stiffener lengths compared with the control model TzE-0.1 W, which failed at a load of 493.95 kN and a displacement of 3.39 mm. The ultimate load decreased to 434.5 kN with 5.4 mm displacement. The model TzE-0.15 W failed at 516.59 kN with a displacement of 3.81 mm and had stiffness (K) and energy absorption (En) values of 312.71 and 2929.33, respectively. Comparing it to the reference model (TzE-0.1 W), increasing the edge web stiffener length from 0.1 to 0.15 of the web resulted in a 4.6% increase in ultimate load and a 54.67% increase in energy absorption, but a 6.86% decrease in stiffness (K). The model TzE-0.2 W failed at an ultimate load of 545.41 kN with a displacement of 3.27 mm and had K and En values of 384.57 and 2974.81, respectively. Comparing it to the TzE-0.1 W model, increasing the edge web stiffener length from 0.1 to 0.2 of the web resulted in a 10.42% increase in load, a 14.54% increase in stiffness (K), and a 57.08% increase in energy absorption (En). The model TzE-0.25 W failed at an ultimate load of 533.06 kN with a displacement of 3.57 mm and had K and En values of 343.76 kN/mm and 3203.12 kN/mm, respectively. Comparing it to the TzE-0.1 W model, increasing the edge web stiffener length from 0.1 to 0.25 of the

web resulted in a 7.92% increase in load, a 2.4% increase in stiffness (K), and a 69.13% increase in energy absorption (En). However, comparing these results to the TzE-0.2 W model showed that increasing the edge web stiffener length from 0.2 to 0.25 of the web resulted in a 2.26% decrease in load and a 10.6% decrease in stiffness (K), but a 7.67% increase in energy absorption (En). The model TzE-0.3 W failed at an ultimate load of 473.37 kN with a displacement of 4.24 mm and had K and En values of 257.41 kN/mm and 3118.6 kN mm, respectively. Comparing it to TzE-0.1 W, the increase in edge web stiffener length from 0.1 to 0.3 of the web resulted in a 4.17% decrease in load and a 23.33% decrease in stiffness (K), despite a 64.7% increase in energy absorption (En). Comparing it to the TzE-0.2 W model, the increase from 0.2 to 0.3 of the web resulted in a 13.2% decrease in load and a 33.1% decrease in stiffness (K), but a 4.83% increase in energy absorption (En). All models had a ductility ratio (Dr) of 3.59% and failed due to local buckling. The TzE-0.2 W model had the highest values for load (P) and stiffness (K), while the TzE-0.3 W model had the lowest values for both P and K but the highest value for En. Overall, using middle web stiffeners improves the structural behavior of CFS columns, with the trapezoidal shape being the most effective. The use of edge web stiffeners also impacts column behavior, but the middle web stiffener has a more significant effect. The optimal approach for achieving the best structural behavior is to use both middle and edge web stiffeners together.

6. Conclusions

This study investigated the behavior of CFS lipped channel columns with different shapes and dimensions of web stiffeners under compression load. The performance of the columns was evaluated using a nonlinear 3-D finite element model, which was verified against experimental test results. The main conclusions drawn from the study are as follows:

(1) The use of web stiffeners significantly improves the performance of CFS columns under compression, increasing their ultimate loads, energy absorption, and ductility ratio.
(2) Among the different shapes of web stiffeners studied, the trapezoidal shape exhibited the best performance in terms of ultimate load and energy absorption. Compared with columns without stiffeners, the trapezoidal stiffeners increased the ultimate load by 47.37% and energy absorption by 177.6%. They also outperformed the triangular and rectangular stiffeners, showing increases of 19.57 and 67.53%, and 15.19 and 92.23%, respectively.
(3) The triangular shape of web stiffeners showed the highest stiffness (K) and ductility ratio (Dr) improvements. Compared with columns without stiffeners, the triangular stiffeners increased the stiffness by 85.63% and the ductility ratio by 155.9%. They also outperformed the rectangular and trapezoidal stiffeners, showing increases of 222.9 and 641.9%, and 208.5 and 320.9%, respectively.
(4) The inclusion of edge web stiffeners further enhanced the performance of the columns, resulting in an average increase in capacity of 18% compared with columns without edge stiffeners.
(5) The ratio between the length of the web stiffener and the web itself was found to be a crucial factor in the structural behavior of the CFS columns. Increasing this ratio up to 0.5 improved the overall performance, but further increases led to a decline in column performance.
(6) In the case of models with edge web stiffeners, a ratio of 0.2 between the length of the edge web stiffener and the web was found to be the most effective. Increasing this ratio beyond 0.2 resulted in a decrease in column efficiency.
(7) Comparing the models with different web stiffener lengths and edge web stiffener lengths, it was observed that the impact of changing the web stiffener length was more significant than changing the edge web stiffener length. The columns with different web stiffener lengths showed an average increase of 1.1% in capacity, 9.61% in stiffness, and 173.6% in ductility ratio compared with the columns with different edge web stiffener lengths.

In conclusion, incorporating web stiffeners, particularly in trapezoidal or triangular shapes, significantly enhances the structural behavior of CFS lipped channel columns under compression. The inclusion of edge web stiffeners provides additional benefits. It is important to carefully consider the ratio between the web stiffener length and the web length to optimize column performance.

Author credit statement

Mahmoud Elnagar: Data curation: Supporting Investigation: Lead Methodology: Equal Supervision: Equal Writing – review & editing: Supporting. Boshra Eltaly: Conceptualization: Lead Investigation:

Supporting Methodology: Lead Supervision: Equal Validation: Supporting Writing – review & editing: Supporting. Dalia Noreldin: Data curation: Lead Investigation: Equal Software: Equal Validation: Equal Writing – original draft: Lead Writing – review & editing: Equal. Ghada M. Hekal: Formal analysis: Supporting Investigation: Supporting Software: Lead Supervision: Equal Writing – original draft: Supporting Writing – review & editing: Lead.

Conflicts of interest

None declared.

References

Ananthi, G.B.G., Ashvini, B., 2019. Experimental theoretical and numerical studies on cold-formed steel stub channel columns with stiffeners. Asian J. Civil Eng. 20, 171–185.

Anbarasu, M., Kanagarasu, K., Sukumar, S., 2014. Investigation on the behaviour and strength of cold-formed steel web stiffened built-up battened columns. Mater. Struct.

Aruna, G., Sukumar, S., Karthika, V., 2019. Behaviour of cold-formed steel built-up closed columns composed by angle profiles. Asian J. Civil Eng. 20, 1037–1048.

Badr, A., Mahmoud, N.S., Salem, F.A., 2022. Studying the behavior of cold-formed steel sections in lightweight buildings. Mansoura Eng. J., (MEJ) 47.

El-Taly, B., El-shami, M., 2021. Structural performance of cold-formed steel face-to-face and back-to-back beams. Int. J. Civ. Eng.

El-Taly, B.A., Fattouh, M., 2022. Optimization of cold-formed steel channel columns. Int. J. Civ. Eng. 18, 995–1008.

Ghannam, M., 2017. Axial load capacity of cold-formed steel built-up stub columns. Int. J. Steel Structures 17, 1273–1283.

Gurupatham, B.G.A., Roy, K., Raftery, G.M., Lim, J.B.P., 2022. Influence of intermediate stiffeners on axial capacity of thin-walled built-up open and closed channel section columns. Buildings 12 (8), 1071.

He, Z., Peng, S., Zhou, X., Yang, G., Schafer, B.W., 2023. Failure characteristics of cold-formed steel built-up sections with web stiffeners under axial and eccentric compression. Thin-Walled Struct. 182 (part B).

Huang, X.H., Yang, J., Liu, Q.F., Li Bai, J.Z., Wang, F.L., Wang, J.H., 2018. A simplified flange-lip model for distortional buckling of cold-formed steel channel-sections with stiffened web. Int. J. Mech. Sci. 136, 451–459.

Li, Q.Y., Young, B., 2023. Experimental and numerical studies on cold-formed steel battened columns. Eng. Struct. 288.

Liu, Z., Liu, H., Chen, Z., Zhang, G., 2018. Structural behavior of cold-walled rectangular steel columns. J. Constr. Steel Res. 147, 277–292.

North American Specification for the design of cold-formed steel structural member. 2007 Edition, American Iron and Steel Institute, October 2007.

Roy, K., Ting, T.C.H., Lau, H.H., Lim, J.B.P., 2018. Nonlinear behaviour of back-to-back gapped built-up cold-formed steel channel sections under compression. J. Constr. Steel Res. 147, 257–276.

Roy, K., Chen, B., Fang, Z., Uzzaman, A., 2022. Axial capacity of back-to-back built-up aluminum alloy channel section columns. J. Struct. Eng. 148, 2.

Ting, T.C.H., Roy, K., Lau, H.H., Lim, J.B.P., 2017. Effect of screw spacing on behavior of axially loaded back-to-back cold-formed steel built-up channel sections. Adv. Struct. Eng. 21, 474–487.